

Numerical Analysis of Temperature and Potential Distributions in Planar-Type SOFC

Masayuki Suzuki*, Koji Fukagata, Naoki Shikazono and Nobuhide Kasagi

*Department of Mechanical Engineering, The University of Tokyo, Japan
E-mail: msuzuki@thtlab.t.u-tokyo.ac.jp, fukagata@thtlab.t.u-tokyo.ac.jp,
shika@thtlab.t.u-tokyo.ac.jp, and kasagi@thtlab.t.u-tokyo.ac.jp

Keywords: Solid oxide fuel cell, Numerical analysis, Potential distribution, Cell design

Abstract: A series of numerical simulation is performed for investigation of the heat and mass transport coupled with electrochemical reactions in a planar-type solid oxide fuel cell (SOFC). The simulation results show that the deterioration of cell output voltage are primarily due to the internal resistance in the interconnector and the activation overpotential of the electrodes. The temperature difference in the cell becomes larger with the increase of cell length. Based on the results, we propose an improved cell design, which uses a material with low electrical resistance and high thermal conductivity. The calculated output voltage of the newly designed cell is about 7 to 10 % higher than that of the conventional cell. Additionally, the maximum temperature of the cell is reduced by 10 to 40 K.

1. Introduction

The solid oxide fuel cell (SOFC) is expected to be a promising energy conversion device because of its high efficiency, flexible fuel adaptability, and possible exhaust-heat utilization. For successful development of SOFCs, it is essential to clarify the physical phenomena occurring inside the cell, such as heat and mass transport and electrochemical reactions. However, it is difficult to experimentally measure all the related parameters under various operating conditions. As is the case of other thermo-fluid devices, numerical simulation should give useful information.

Detailed numerical simulations on the cell performance have recently been reported for planar (Yakabe et al., 2001) and tubular type (Li and Chuy, 2003), (Campanari and Iora, 2004) SOFCs. However, effects of the configuration, such as dimensions, and the material of the cell components, have not been sufficiently studied. An exception is the work by Chan et al. (2001), who investigated the cell performance focusing on the electrolyte and electrode thicknesses. Through the simulation, they show that performance of the anode-supported SOFC is superior to that of electrolyte or cathode supported SOFC. However, they did not take into account the interconnector, which should also have considerable influence on the cell performance.

In the present study, numerical simulations are performed of a planar-type SOFC. A special focus is laid upon the voltage drops and the temperature distribution in the cell. Effects of the interconnector on those are also evaluated. Based on the simulation results, an improved design of the cell is suggested, and the performance of this newly designed cell is compared to that of the conventional cell.

2. Simulation model and governing equations

We assume a sufficiently wide multi-layered stack, as shown in Fig. 1(a). Since the field is spatially periodic with a unit noted by the dashed line, only one unit is taken as a simulation domain, as shown in Fig. 1(b). The unit is composed of an electrolyte, a cathode and an anode sandwiched between air and fuel conduits. Simulation is repeated for different cell lengths in order to investigate the size effect. The physical properties of the solid component material are shown in Table 1.

The assumed operating condition is shown in Table 2. Completely reformed methane (S/C=2.5) is chosen as a fuel. The molar ratio of the fuel gas composition at the inlet is $H_2 : H_2O : CO_2 = 8:1:2$. The average current density in the electrolyte is kept constant.

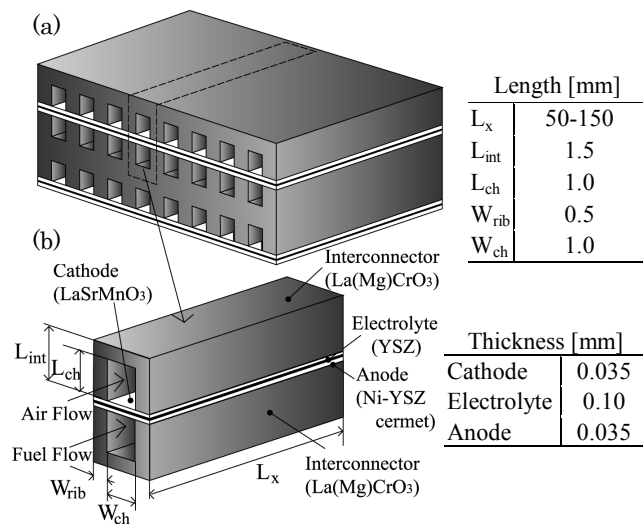


Fig. 1 (a) Schematic of planar-type SOFC;
(b) computational domain.

Table 1 Physical properties of cell material.

Component	Resistivity [Ωcm]	Thermal Conductivity [W/mK]
Interconnector	0.50	6.0
Cathode	0.013	11.0
Electrolyte	$10e^{(10092(1/T-1/1273))}$	2.7
Anode	0.0010	6.0

(Onda et al., 2000)

Table 2 Operating conditions of SOFC.

Utilization rate of oxygen and hydrogen	0.3, 0.85
Inlet temperature and pressure	1073 K, 1.0 atm
Electrolyte average current density	0.3 A/cm ²

The governing equations of the thermo-fluid field (i.e., the continuity, momentum, and energy equations) and the transport equations of five chemical species (O₂, N₂, H₂, H₂O and CO₂) can be written as

$$\frac{\partial \rho}{\partial t} + \nabla \cdot (\rho \mathbf{u}) = 0, \quad (1)$$

$$\frac{\partial (\rho \mathbf{u})}{\partial t} + \nabla \cdot \{(\rho \mathbf{u}) \mathbf{u}\} = -\nabla P + \nabla \cdot \left[\mu \left(\nabla \cdot \mathbf{u} + \frac{\partial u_j}{\partial x_i} - \frac{2}{3} \delta_{ij} \frac{\partial u_k}{\partial x_k} \right) \right], \quad (2)$$

$$\frac{\partial (\rho h)}{\partial t} + \nabla \cdot (\rho \mathbf{u} h) = \nabla \cdot (\lambda \nabla T), \quad (3)$$

$$\frac{\partial (\rho Y_i)}{\partial t} + \nabla \cdot (\rho \mathbf{u} Y_i) = \nabla \cdot (\rho D_{im} \nabla Y_i). \quad (4)$$

where, \mathbf{u} is the fluid velocity, and h , ρ , μ , λ are enthalpy, density, viscosity, and thermal conductivity of fluid, respectively. D_{im} is mass diffusion coefficient of gas species i in the mixture. These equations are solved by using the finite different method (FDM).

The fields are assumed, for simplicity, to have variations only in the streamwise and the perpendicular directions, as shown in Fig. 2. The chemical reactions, which take place on the electrolyte and electrode surfaces, are incorporated as mass fluxes of oxygen. All the outer wall boundaries are treated as adiabatic. The heat generated in the cell is removed out of the cell by convection. The physical properties of the fluid are treated as functions of the local fluid temperature and the fraction of gas species. For efficient computation of the thermo-fluid field with the variable physical properties, the low-Mach number approximation (Majda and Sethian, 1985) is adopted.

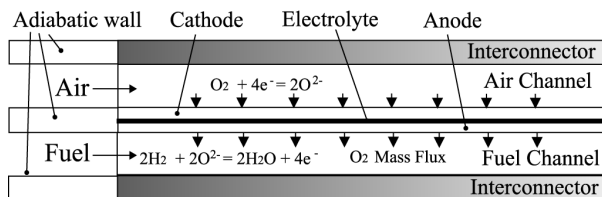


Fig. 2 Computational model for the calculation of the heat and mass transport in the cell.

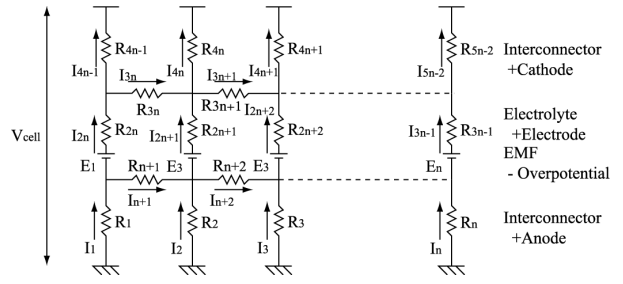


Fig. 3 Equivalent electrical circuit.

The electromotive force (EMF) generated in the cell, E is given by the Nernst equation, which reads,

$$E = -\frac{\Delta G_{H_2O}^o}{2F} + \frac{RT}{4F} \ln \left\{ \frac{p_{H_2,an}^2 p_{O_2,ca}}{p_{H_2O,an}^2} \right\}. \quad (5)$$

The activation overpotentials in the cathode and anode are calculated by using the modified Butler-Volmer law, i.e.:

$$i_e = \frac{RT}{4F} s_{ca} \left\{ \exp\left(\frac{2FV_{act,ca}}{RT}\right) - \exp\left(-\frac{2FV_{act,ca}}{RT}\right) \right\}, \quad (7)$$

$$i_e = \frac{RT}{3F} s_{an} \left\{ \exp\left(\frac{2FV_{act,an}}{RT}\right) - \exp\left(-\frac{FV_{act,an}}{RT}\right) \right\}, \quad (8)$$

$$s_{ca} = 62.7 \times 10^6 \exp(-136000/RT) p_{O_2,ca}^{0.5}, \quad (9)$$

$$s_{an} = 125.6 \times 10^{10} \exp(-138000/RT) p_{O_2,an}^{0.15}. \quad (10)$$

where s_{ca} and s_{an} denote the interface conductivities of the cathode and anode, respectively. The local current density, i , is computed by using an equivalent circuit including the internal resistance, the EMF, and the overpotential in the cell, as shown in Fig. 3. Based on these electrochemical reactions, the amount of local heat generation is determined and fed back to the simulation of the thermo-fluid field.

3. Simulation results and discussions

Distributions of the molar fractions of oxygen, hydrogen, and water vapor in the cell are shown in Fig. 4. For all species, a large concentration gradient can be found in the gas flow direction. The concentration gradient for the perpendicular direction is much smaller. Namely, the diffusion is very fast. Therefore, it should be difficult to improve the cell performance by controlling the local gas concentration.

Figure 5 shows the contributions to the total voltage drop at different longitudinal positions. The cell length is 150 mm. It reveals that the dominant factors for the voltage loss are the activation overpotential (V_{act}) and the ohmic loss due to the internal resistance of the interconnector ($V_{i,int}$). Although the resistivity of the interconnector material is much smaller, the current

path is longer and narrower than that of the electrolyte. As a result, the voltage loss in the interconnector becomes larger than that in the electrolyte. In fact, the internal resistance of the cathode ($V_{r,ca}$) and anode ($V_{r,an}$), and the concentration overpotential (V_{con}) of both electrodes are negligibly small.

Previous studies mainly focused on the voltage drop due to the activation overpotential and the internal resistance. The present results indicate that the interconnector resistance may also be a significant factor for the voltage drop, and higher performance is expected if this internal resistance can be reduced.

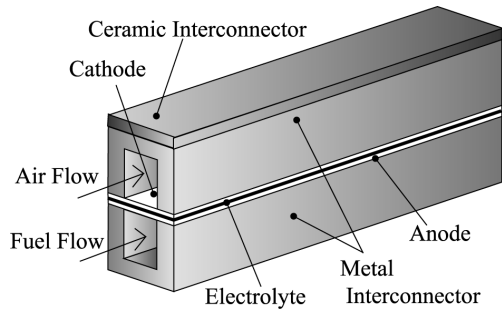


Fig. 7 Improved design of the cell.

Table 3 Physical properties of interconnector.

Material	Resistivity [Ωcm]	Thermal Conductivity [W/mK]
Ceramic	0.50	6.0
Metal	0.10	30.0

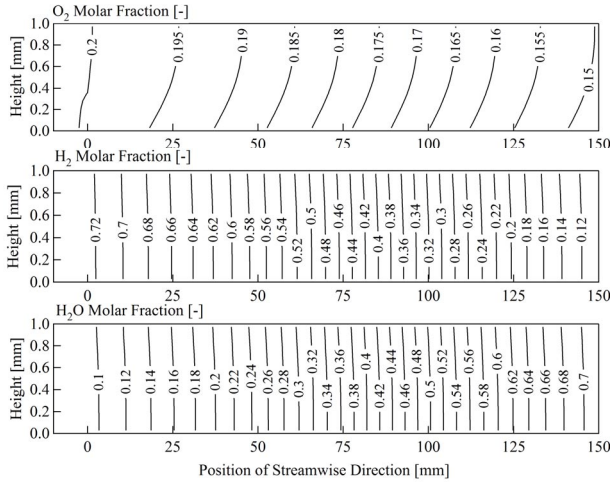


Fig. 4 Molar fraction of gas species (O_2 , H_2 , H_2O) in the cell.

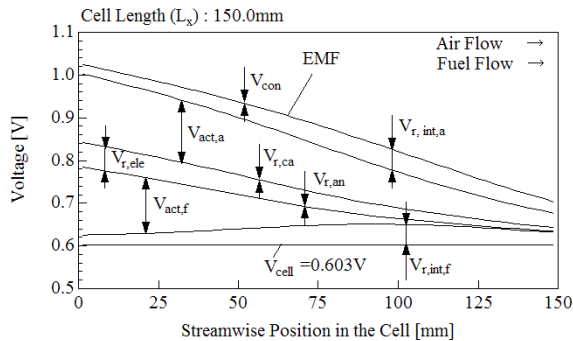


Fig. 5 Distributions of EMF and loss factors in the conventional design cell.

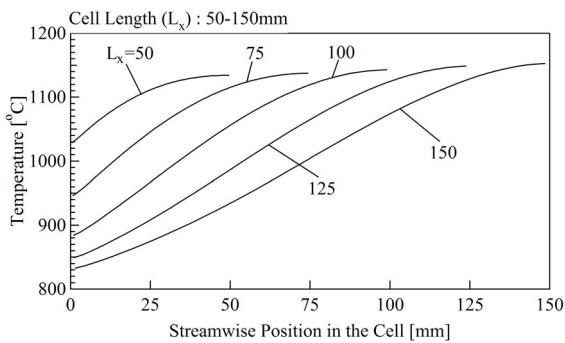


Fig. 6 Electrolyte temperature distribution of the conventional design cell.

The electrolyte temperatures in the cells of different lengths are shown in Fig. 6. The temperature distribution in the cell is largely affected by the heat conduction in the solid walls. In shorter cells, the heat generated near the cell outlet is well diffused toward the inlet region. However, with increasing of the cell length, this effect decreases and the temperature difference between the inlet and outlet becomes larger.

Based on the results above, an improved design of cell is proposed as shown in Fig. 7. In order to reduce the internal resistance, and to promote the heat conduction in the walls, the material of the conduits is replaced by metal alloy or porous metal alloy. In the case of porous material, a thin ($100\ \mu\text{m}$) ceramic interconnector is used only for the gas sealing. The assumed resistivity and thermal conductivity of this metal interconnector are $0.1\ \Omega\text{cm}$ and $30\ \text{W/mK}$, respectively.

As shown in Fig. 8, the output voltage with this improved design increases about 7 to 10 % and becomes less sensitive to the cell length compared to the conventional design. Distributions of the EMF, the output voltage, and the loss factors are shown in Fig. 9. Owing to the lower electrical resistance, the ohmic loss in the interconnector is almost negligible. In addition, the activation overpotential and the electrolyte internal resistance also decrease.

This additional reduction can be explained by the temperature distribution, as shown in Fig. 10. The temperature is more homogeneous due to the enhanced heat conduction in the solid walls, becomes less sensitive to the cell length, and keeps high average value. As a result, the activation overpotential and the electrolyte internal resistance are reduced, because they strongly depend on the temperature. Consequently, the cell output voltage becomes higher. Additionally, the heat generation in the cell becomes smaller, and the maximum temperature is reduced by 10 to 40 K.

In the present study, simulations are carried out only for high cell operating temperature. However, the method used here for the improvement of cell performance should also be effective for the operation under an intermediate temperature, which may be more suitable for the metal component.

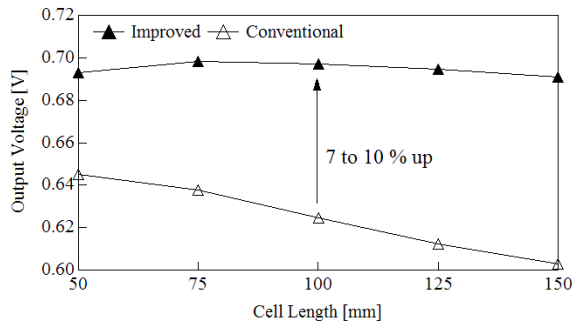


Fig. 8 Dependence of output voltage on cell length.

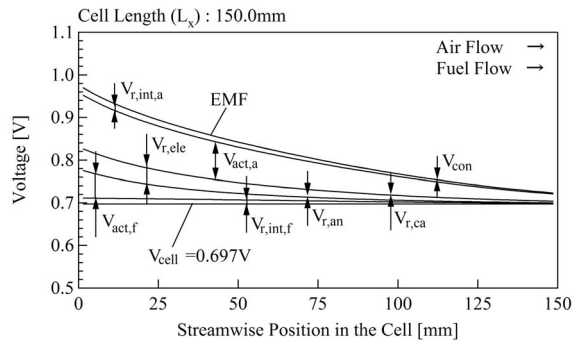


Fig. 9 EMF and loss factors distribution in the improved cell.

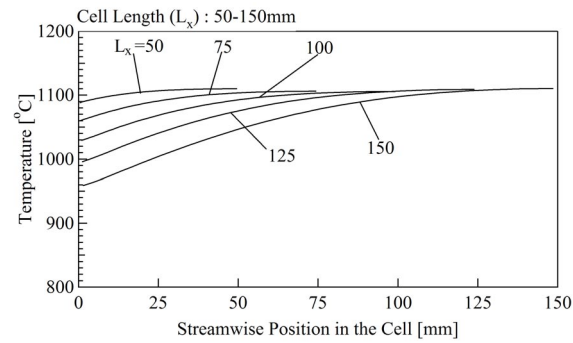


Fig. 10 Electrolyte temperature distribution in the improved cell.

4. Conclusions

Through the numerical simulation of a planar-type SOFC, we found that the interconnector plays an important role for the cell output voltage and temperature distributions. The internal resistance of the interconnector is one of the main factors for the deterioration of cell output voltage. Therefore, by employing materials with higher electric conductivity, the cell output voltage can be improved drastically.

In addition, the heat conduction in the wall is also enhanced to reduce the temperature difference in the cell. By this change, both the activation overpotential and the electrolyte internal resistance can be reduced without changing the thickness, material or microstructure of the electrolyte and the electrode. Furthermore, due to the reduction of loss in the cell, the maximum temperature is kept by 10 to 40 K lower than that in the conventional cell under present operating conditions.

Acknowledgement

This research is supported through the CREST project, "Micro Gas Turbine and Solid Oxide Fuel Cell Hybrid Cycle for Distributed Energy System", by Japan Science and Technology Agency (JST).

Nomenclature

E	Electromotive force (EMF) (V)
F	Faraday constant : 9.649×10^4 C/mol
ΔG°	Standard Gibbs' free energy change for reaction (J/mol)
h	Enthalpy (J/kg)
i	Current density (A/m^2)
P	Pressure (Pa)
p	Partial pressure (Pa)
R	Gas constant : 8.314 J/mol K
T	Temperature (K)
u	Fluid velocity (m/s)
V_{con}	Concentration overpotential (V)
V_r	Ohmic overpotential (V)
V_{act}	Activation overpotential (V)
V_{cell}	Cell output voltage
Y_i	Mass fraction of the gas component i (-)

Subscript

an	Anode
ca	Cathode
ele	Electrolyte
H_2	Hydrogen
H_2O	Water vapor
int	Interconnector
O_2	Oxygen

References

- Campanari, S., and Iora, P., 2004, Definition and sensitivity analysis of a finite volume SOFC model for a tubular cell geometry.
- Chan, S. H., et al., 2001, A Complete polarization model of a solid oxide fuel cell and its sensitivity to the change of cell component thickness, J. Power Sources, Vol. 93, pp. 130-140.
- Li, P. W., and Chuy, M. K., 2004, A Numerical Model Coupling the heat and Gas Species' Transport Processes in a Tubular SOFC, J. Heat Transfer, Vol. 124, pp. 219-229.
- Majda, A., and Sethian, J., 1985, The Derivation and Numerical Solution of the Equations for Zero Mach Number Combustion, Chemical Science and Technology, Vol. 42, pp.185-205.
- Onda, K., et al., 2000, Performance analysis of planar-type unit SOFC considering current and temperature distributions, Solid State Ionics, Vol. 132, pp. 297-308.
- Yakabe, T., et al., 2001, 3-D model calculation for planar SOFC, J. Power Sources, Vol. 102, pp. 144-154.